Accepted Manuscript

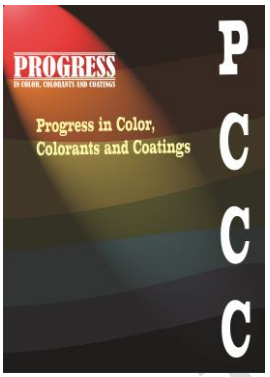

Title: Enhanced Surface Modulation of CNT and CN-PS Nanocomposites via Plasma Treatment

Authors: R. Alsayed, K. Zainulabdeen1, R. N. Abed, R. T. Abdulla, M. Al-Baidhani, A. A. Rashad, H. Hashim, B. M. Abood, R. Noaman, K. A. Aadim, A. H. Shaker, T. S. Gaaz, S. A. Ismael, E. A. Yousif

Manuscript number**: PCCC-2509-1445**

To appear in: Progresss in Color, Colorants and Coatings

Received: 31 August 2025

Final Revised: 16 October 2025

Accepted: 18 October 2025

Please cite this article as:

R. Alsayed, K. Zainulabdeen, R. N. Abed, R. T. Abdulla, M. Al-Baidhani, A. A. Rashad, H. Hashim, B. M. Abood, R. Noaman, K. A. Aadim, A. H. Shaker, T. S. Gaaz, S. A. Ismael, E. A. Yousif, Enhanced Surface Modulation of CNT and CN-PS Nanocomposites via Plasma Treatment, Prog. Color, Colorants, Coat., 19 (2026) XX-XXX.
DOI: 10.30509/pccc.2025.167654.1445

Enhanced Surface Modulation of CNT and CN-PS Nanocomposites via Plasma Treatment

R. Alsayed[1], K. Zainulabdeen[1], R. N. Abed[2], R. T. Abdulla[3], M. Al-Baidhani[3], A. A. Rashad[1], H. Hashim[4], B. M. Abood[5], R. Noaman[5], K. A. Aadim[6], A. H. Shaker[7], T. S. Gaaz[8], S. A. Ismael[4], E. A. Yousif[1*]

[1.] Department of Chemistry, College of Science, Al-Nahrain University, P.O. Box: 64021, Jadriyah, Baghdad, Iraq

[2.] Department of Mechanical Engineering, College of Engineering, Al-Nahrain University, P.O.Box: 64040, Jadriyah, Baghdad, Iraq.

[3.] Department of Physics, College of Science, Al-Nahrain University, P.O. Box: 64021, Jadriyah, Baghdad, Iraq

[4.] Medical Physics Department, College of Science, Al-Nahrain University, P.O. Box: 64021, Jadriyah, Baghdad, Iraq

[5.] Chemical and Petrochemical Research Center, Corporation of Research and Industrial Development, Ministry of Industry and Minerals, P.O. Box: 47182, Baghdad, Iraq

[6.] Institute of laser for postgraduate studies, University of Baghdad, P.O. Box: 47134, Baghdad, Iraq.

[7.] Department of Physics, College of Science, University of Baghdad, P.O. Box: 47131, Baghdad, Iraq.

[8.] Department of Prosthetics and Orthotics Engineering, College of Engineering and Technologies, Al-Mustaqbal University, P.O. Box: 100, Babylon, Iraq

Email: emad.yousif@nahrainuniv.edu.iq

Abstract

New spectrally nanocomposite films have been developed for high absorption performance. The polystyrene (PS) was dissolved in THF and blended with fixed concentrations of carbon nanotubes (CNT) and carbon nanofibers (CN) (5 wt. % CNT, 5 wt. % CN, and 2.5 wt. % CNT+CN) via the casting technique to produce nanocomposite films. Polymer nanocomposite films have been developed to create an economical coating that reinforces the poly (styrene) matrix. The coating exhibits high absorptivity; the optical properties were computed over a wavelength range of 250-1350 nm at 30 °C. The transmittance and reflectance were decreased, skin depth and optical density were increased, and the absorbance coefficient and dielectric constant were increased. The direct and indirect energy gap (E_g) of the films has decreased from 2.8 to 2.4 eV and from 3.4 to 2.9 eV after adding CNT with CN. The Urbach energy (E_u) has increased from 1.24 to 2.71 eV. The XRD test confirms that the films had amorphous structures. The SEM analysis was used to show the surface morphology of thin films. Consequently, the atomic force microscopy (AFM) measurements indicated an increase in surface roughness (SR) from 5.19 to 14.5 nm for the doped PS thin films, and the root mean square (RMS) roughness increased from 6.65 to 16.6 nm. These modified PS nanocomposite thin films find potential applications in various industries, including air transport components, light-emitting diodes, laser sensors, UV energy shielding, light-harvesting devices, memory devices, and light-conversion technologies.

Keywords: PS, DBD plasma, Nanocomposite PS/CNT+CN, Optical properties, AFM and SEM analysis

1. Introduction

Polystyrene (PS), a widely used thermoplastic polymer renowned for its cost-effectiveness, chemical inertness, and processability, faces significant limitations in mechanical strength and optical clarity, which restrict its advanced applications [1-3] as shown in Figure 1. To address these limitations, recent studies have investigated the incorporation of carbon-based nanomaterials into PS matrices, resulting in nanocomposites with notably improved properties. For example, virtual simulations and experimental tests show that adding 0.5 wt.% multi-walled carbon nanotubes (MWCNTs) increases tensile strength by approximately 35% and Young's modulus by around 50% compared to pure PS, due to better stress transfer and nanofiller dispersion. Similarly, nano-carbon (NC) additives at 1.0 wt.% show a 20% reduction in UV degradation while maintaining over 90% optical transparency in thin films, as predicted by density functional theory (DFT) analyses [5]. These advancements highlight the potential of carbon nanomaterials to customize PS for high-performance applications in packaging, optoelectronics, and structural components. However, challenges in scalable dispersion and interfacial compatibility remain key areas for future research [6-7]. CNTs, characterized by their high aspect ratio, exceptional electrical conductivity, and mechanical strength, have been widely studied for their reinforcing capabilities in polymer matrices [5]. When evenly dispersed within PS, CNTs can significantly modify the composite's optical properties, including its absorption coefficient, refractive index, and optical bandgap. Similarly, the addition of NC can affect the dielectric constant and conductivity of the resulting nanocomposite films. Recent studies have shown that incorporating CNTs and NC into PS results in decreased reflectance and transmittance,

along with increased surface roughness and Urbach energy, indicating greater disorder and more localized states within the band structure [6-10].

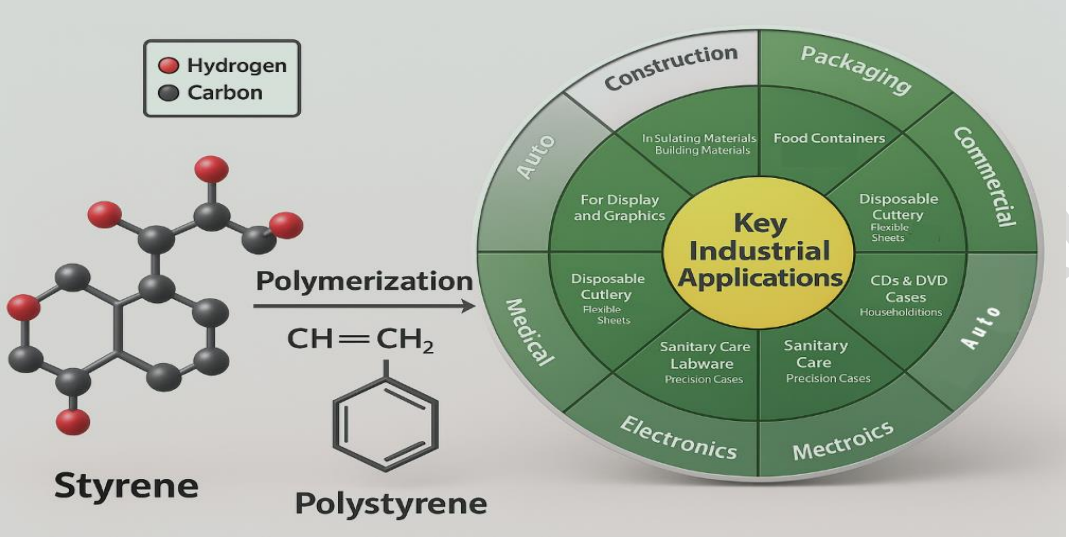

Figure 1. Polystyrene preparation steps and applications.

Surface modification techniques, particularly plasma treatment, have been employed to tailor the properties of polymer nanocomposites further [11, 12]. Plasma treatment adds functional groups to the surface of CNTs, improving their dispersion in the polymer matrix and enhancing interfacial adhesion. For example, plasma-functionalized multi-walled carbon nanotubes (MWCNTs) have demonstrated improved compatibility with PS matrices, resulting in enhanced optical, thermal, and electrical properties of the nanocomposite films. Additionally, plasma treatments can alter the surface energy and morphology of the nanocomposite films, resulting in changes in wettability and optical properties as shown in Figure 2. [13-18].

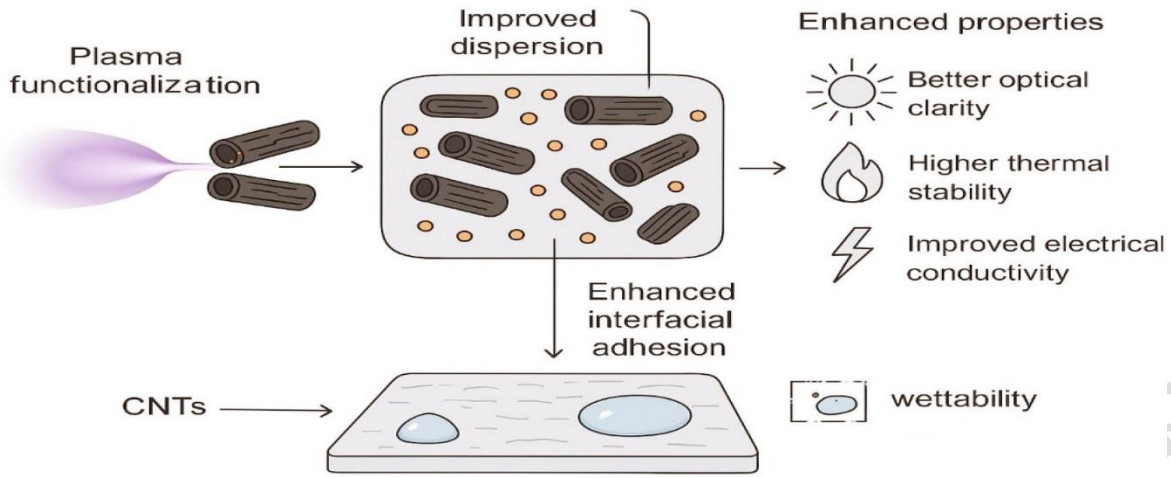

Figure 2. Surface modification techniques by plasma.

The relationship between the incorporation of CNT/NC and the effects of plasma treatment on the optical properties of PS nanocomposites remains an active area of research. Understanding how plasma-induced surface modifications affect molecular structural changes and, in turn, the optical properties of these nanocomposite films is essential for their use in optoelectronic devices, sensors, and other advanced technologies [19, 20].

This study aims to examine the optical properties of CNT and NC-infused PS nanocomposite films and evaluate the effects of plasma treatment on their surface molecular structure. By linking changes in optical parameters to surface morphological modifications following plasma exposure, we aim to elucidate the mechanisms underlying the observed improvements and to provide insights into the design of PS-based nanocomposites with tailored optical properties. The novelty of this manuscript lies in grafting PS with CNT and CN, in single or combined forms, and in irradiating them with laser radiation to modify the PS lattice structure, thereby achieving high absorption. This property is utilized as a valuable parameter in various optoelectronic applications.

2. Experimental

The current study builds upon our previously reported findings on PS/CNT composites, focusing on the evaluation of plasma surface modification's role in enhancing optical functionality [21]. The synthesis process for the polymer involves incorporating 0.05 CN, 0.05 CNT, and a mixture of 0.025 CN + 0.025 CNT into the polymer matrix to produce I1, I2, and I3, respectively, along with a blank PS (I0) sample as a reference. Table 1 shows the percentage of the CN and CNT that were used to dope the PS.

Table 1. The samples are used to constitute the nanocomposite films.

No.	Samples	PS (g)	CN %	CNT %
1	I0	1	-	-
2	I1	1	0.05	-
3	I2	1	-	0.05
4	I3	1	0.025	0.025

The project includes exposing PS nanocomposite films to a cold plasma system operating at up to 10 kV and up to 50 Hz. Samples were placed between two discs, with a 2 mm distance separating them.

3. Results and Discussion

The outcomes of the PS nanocomposite films incorporating CNT and CN, following exposure to DBD plasma rays, include computed values for absorbance, reflectance, extinction coefficient, refractive index, dielectric constant (both real and imaginary), skin depth, energy gap, and Urbach energy for both the blank PS and the nanocomposite thin film PS/CN+CNT as shown in Figures 3.

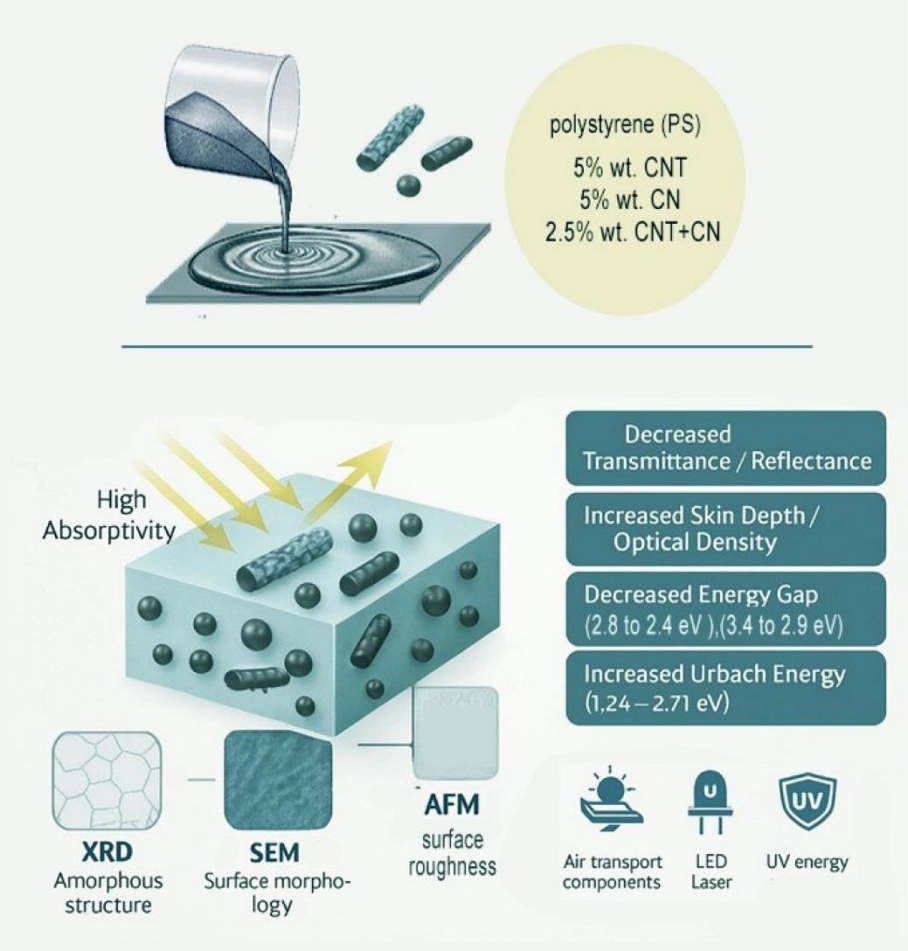

Figure 3. PS nanocomposites and their characterization methods.

3.1. XRD analysis

The crystalline structure was examined using X-ray diffraction. Figure 4 presents the X-ray diffraction (XRD) patterns of the samples after dielectric barrier discharge (DBD) plasma treatment. As shown, the blank PS sample (I_0) exhibits no significant changes in its diffraction pattern before and after plasma exposure, indicating that the DBD plasma has a negligible effect on its crystalline structure. For the CN-doped PS samples, I1 shows a broad diffraction band spanning approximately 15°-25° (2θ) and extending continuously across the wavelength range, suggesting a high degree of crystallinity. Sample I2 shows a small hump and a broad peak in the regions of 15°-25°, while sample

I3 exhibits a single diffuse hump centered between 15° and 25°, and has a hump like that of I2. These broad features, characterized by sharp peaks, are indicative of a semi-crystalline structure in the nanocomposite thin films [21].

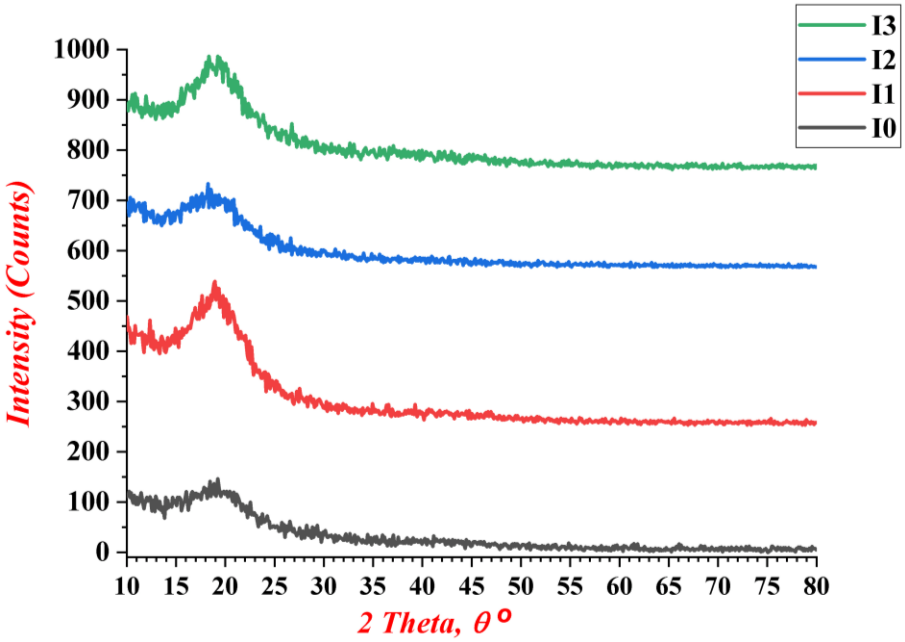

Figure 4. shows the XRD analysis of patterns I0, I1, I2, and I3.

3.2. EDX analysis of the PS nanocomposite thin films

The EDX analysis of the PS nanocomposite films is presented in Table 2, which lists the elemental composition of the CN and CNT nanoparticles prepared from burnt papyrus reed in the laboratory. These elements show the main components are carbon, oxygen, and sodium, which have the percentages (28.0, 38.0, and 24.8 %); the other elements are microscopic compared with the main components. Figure 5 shows the elemental composition over the electro-voltage range, representing the spectrum incident on the CN and CNT samples as powders. After that, Figure 6 shows the elemental compositions in colors, with each element assigned a distinct color to represent its composition in the composite.

Table 2. The compositions of the elements that constitute the CN and CNT

Element	Weight %	Atomic % Error	Atomic %	Weight % Error
C	28.0	0.2	38.9	0.2
O	38.0	0.2	39.7	0.2
Na	24.8	0.1	18.0	0.1
Mg	0.1	0.0	0.1	0.0
Al	0.1	0.0	0.1	0.0
Si	2.5	0.0	1.5	0.0
S	0.3	0.0	0.1	0.0
Cl	0.0	0.0	0.0	0.0
Ca	0.3	0.0	0.1	0.0
Fe	0.7	0.0	0.2	0.0
Zn	5.2	0.0	1.3	0.1

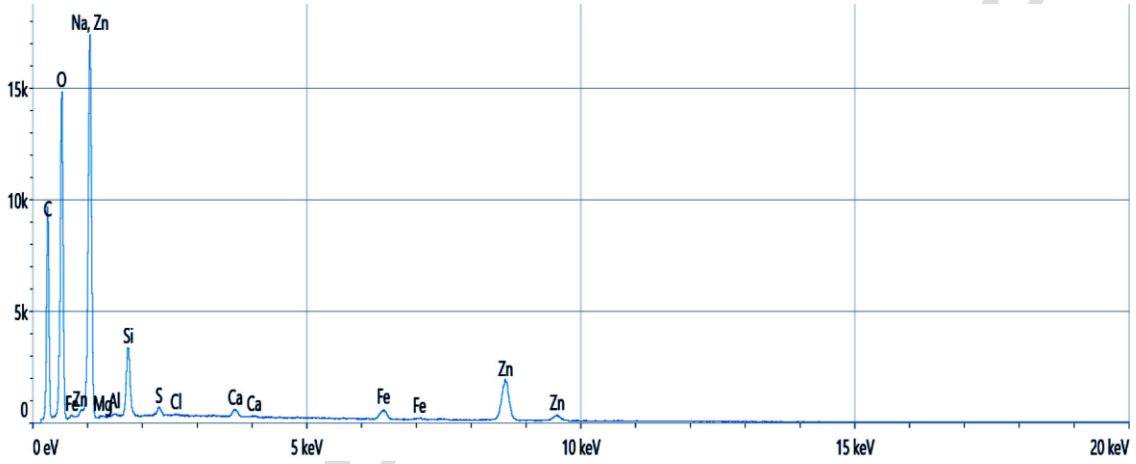

Figure 5. The elemental composition of the electron volt spectrum.

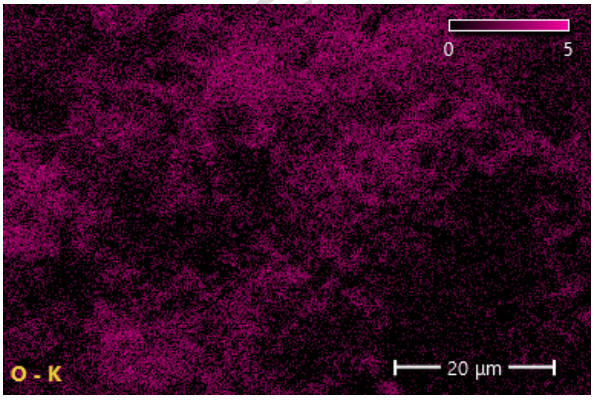

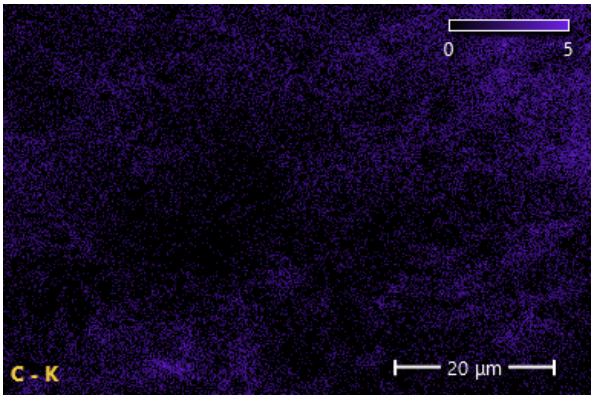

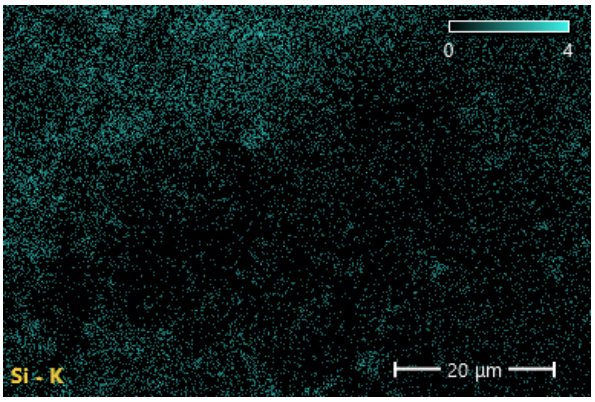

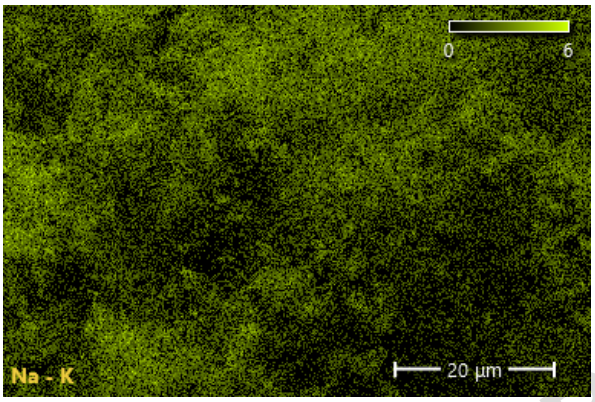

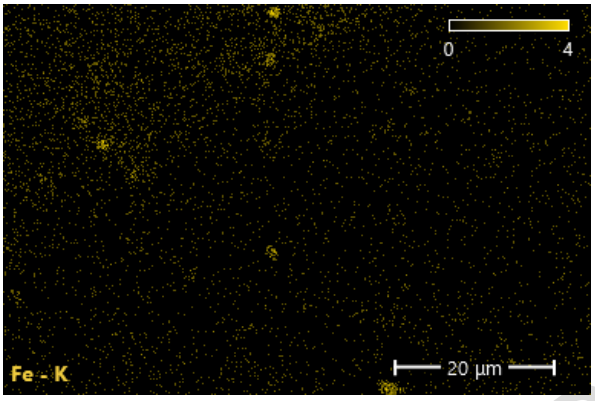

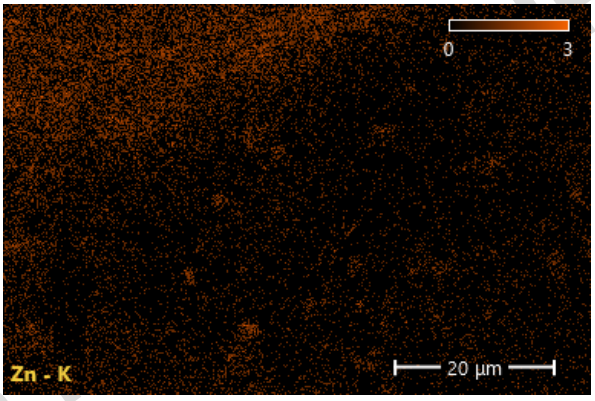

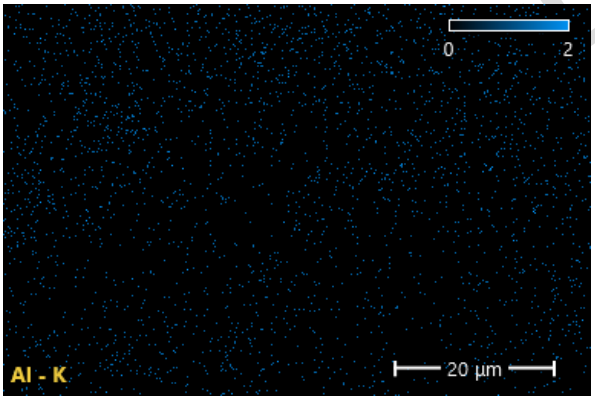

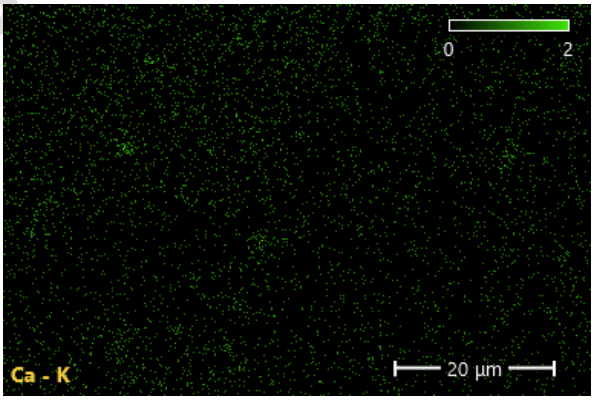

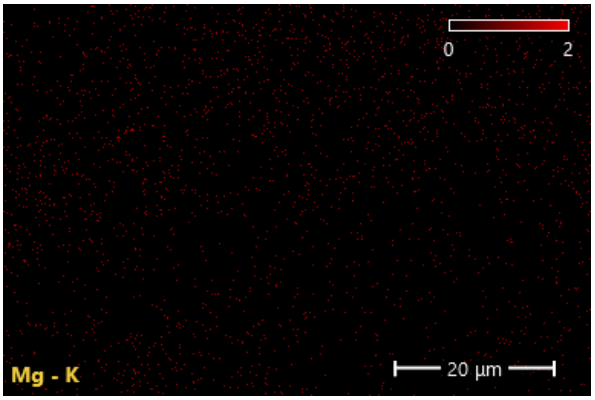

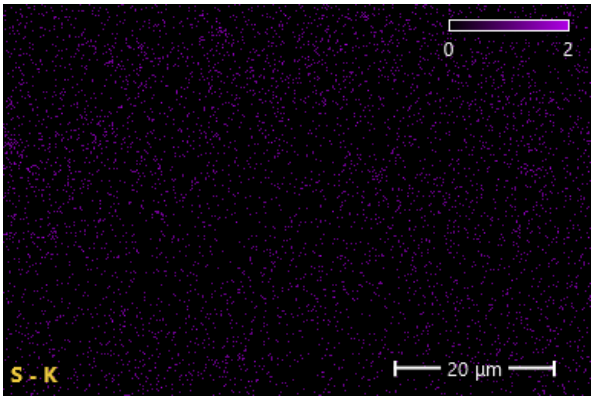

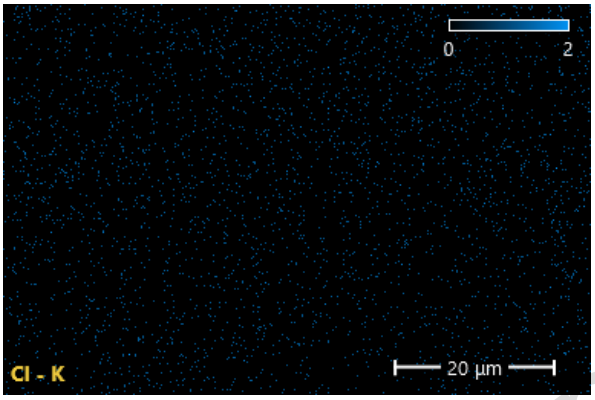

Figure 6 shows the element color for the elemental composition in the composite.

3.3. Optical properties of the nanocomposite films after exposure to DBD plasma

The reflectance spectra of the PS nanocomposite thin films I0 (blank PS), I1, I2, and I3 are presented in Figure 7. As shown, all samples exhibit high reflectance values in the ultraviolet (UV) region, which progressively decrease as the wavelength extends into the visible and infrared (IR) regions. At $\lambda \geq 450$ nm, the reflectance of the I1 sample declines to 0.16 units of reflectance, and it has a lower value than the other samples of the nanocomposite films. Beyond the visible range ($\lambda \geq 750$ nm), the reflectance curves level off and remain relatively constant as the wavelength increases. Notably, samples I2 and I3 exhibit lower overall reflectance than I0 and I1. This reduction is attributed to the incorporation of carbon nanomaterials (CN and CNT) into the PS matrix, combined with dielectric barrier discharge (DBD) plasma treatment, which appears to modify and reorganize the surface morphology and internal structure of the films, thereby enhancing light absorption and reducing surface reflection [22, 23].

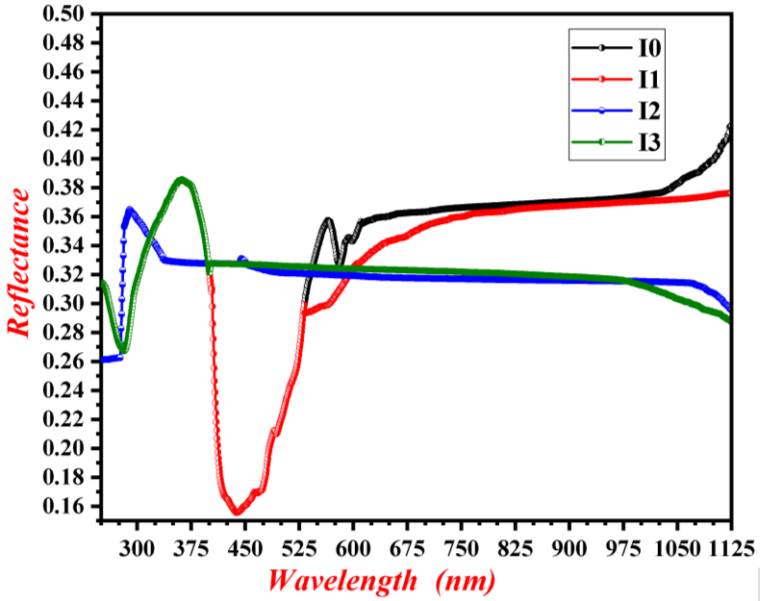

Figure 7. Reflectance test of the PS nanocomposite films I0, I1, I2, and I3.

Figure 8 displays the absorption coefficient (α) as a function of wavelength for the PS nanocomposite thin films I0, I1, I2, and I3. The absorption coefficient was calculated using the absorbance data obtained from UV-Vis spectroscopy and the measured thickness of each film, according to equation 1 [24]:

$$\alpha = 2.303 * \frac{A}{t} \quad \text{..... (1)}$$

where α is the absorption coefficient (cm^{-1}), A is the absorbance, and t is the film thickness (cm).

As shown in Fig. 8, all samples exhibit relatively high initial absorption coefficients in the UV region, which decrease gradually with increasing wavelength. This trend indicates strong photon absorption at lower wavelengths, followed by a reduction in absorption in the visible and near-infrared regions. At $\lambda \geq 450$ nm, the absorption coefficient of the I1 sample increases to 120 cm^{-1}, and it has a higher value than the I3 sample of the nanocomposite films compared to the I0 sample of the blank PS.

The incorporation of carbon nanotubes (CNT) and carbon nanostructures (CN) into the

PS matrix, combined with dielectric barrier discharge (DBD) plasma treatment, appears to alter the electronic structure and morphology of the films. These modifications contribute to the observed variation in absorption behavior, supporting the potential of these nanocomposites for enhanced optical performance [25].

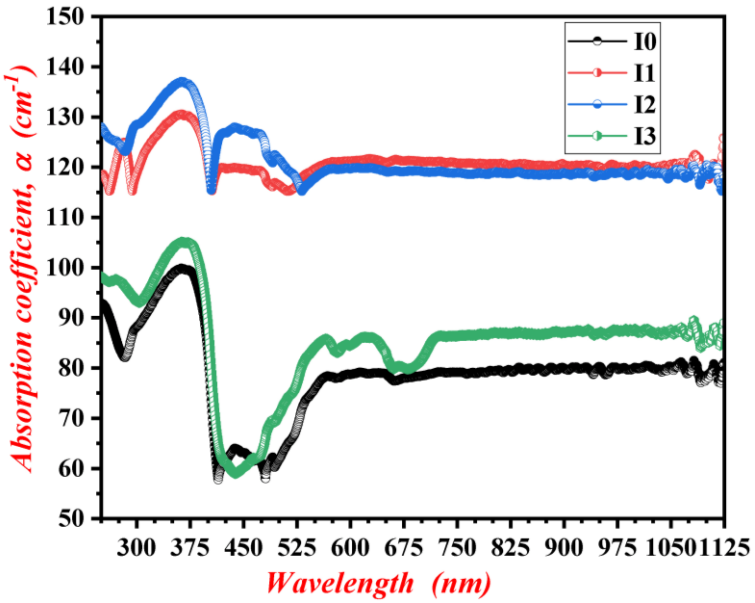

Figure 8. Absorption coefficient (α) of the PS nanocomposite films I0, I1, I2, and I3

Figure 9 illustrates the transmittance values (T) for the PS nanocomposite thin films I0, I1, I2, and I3. It is clearly shown that the transmittance of the PS nanocomposite thin films is reduced after the introduction of CNT and CN into the PS matrix using DBD plasma. Furthermore, the results indicate that I1 has a lower transmittance value than the others [26].

The I1 sample has the highest transmittance, at 61%. In comparison, I2 and I3 have transmittance values of 49% and 57%, respectively. This is in contrast to the I0 of the blank sample of PS, which has a transmittance value of 63%.

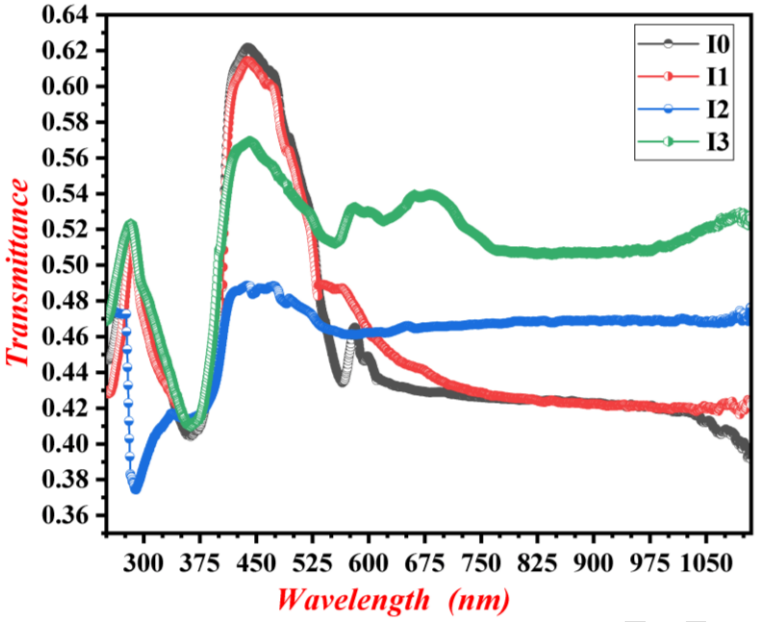

Figure 9. Transmittance of the PS nanocomposite films I0, I1, I2, and I3

The skin depth (x) is illustrated in Figure 10, where its values are arranged as follows: I0, I1, I2, and I3, Consequently, the skin depth values are contingent upon the film thickness, and the ratio of the wavelength with the extinction coefficient, therefore, the skin depth (x) can be computed from equation 2 [27]:

$$x = \frac{\lambda}{2\pi k} \quad \text{..... (2)}$$

So, λ is the wavelength and its unit (nm), and k is the extinction factor.

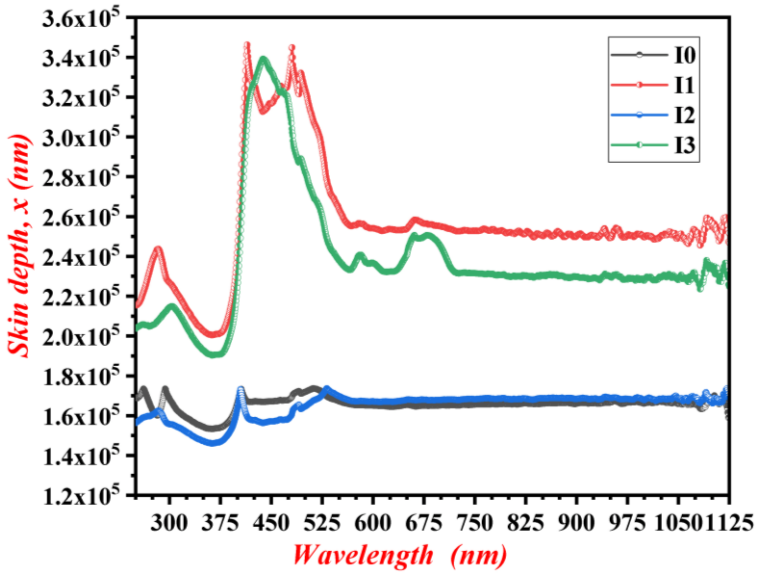

Figure 10. Skin depth (*x*) of the PS nanocomposite films I0, I1, I2, and I3.

Figure 10 reveals that the skin depth of the PS nanocomposite thin films increases after adding CNT and CN to the PS matrix via DBD plasma, resulting in a structure that shows a slight increase and continues to increase steadily with increasing wavelength along the axis. At $\lambda \geq 450$ nm, the skin depths of the I1 sample increase to 3.4 × 10 ^5 nm, and the I3 sample has a value of 3.3 × 10 ^5 nm, where these samples outperform the I2 sample, which has a value of 1.6 × 10 $^{\wedge 5}$ nm for the nanocomposite films. Therefore, the composite yields high absorption values for the nanocomposite thin films, and the I1/I3 nanocomposite films outperform the others compared with the blank PS [28].

The refractive index (*n*) for the PS nanocomposite thin films I0, I1, I2, and I3 illustrated in Figure 11, is regarded as a very important parameter for the electronic nature of the electronic applications. Therefore, it is contingent upon the reflectance and extinction coefficients and can be derived from equation 3 [29]:

$$n = \left[\frac{1+R}{1-R}\right] + \sqrt{\frac{4R}{(1-R)^2} - k^2} \quad \ldots\ldots\ldots\ldots\ldots\ldots (3)$$

where (*n*) denotes the refractive index, (*R*) represents the reflectance values, and (*k*)

signifies the extinction factor values.

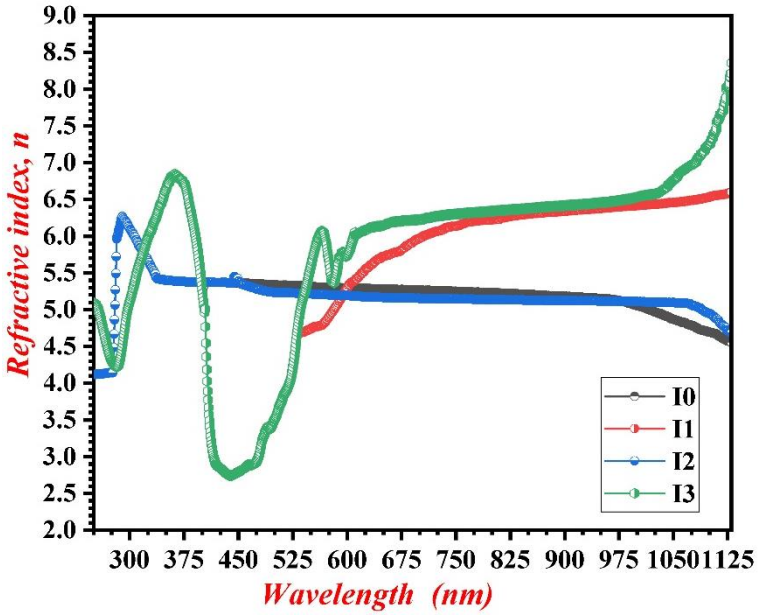

Figure 11. Refractive index (*n*) of the PS nanocomposite films I0, I1, I2, and I3.

As shown in Figure 11, the refractive index of the PS nanocomposite thin films increased after adding CNT and CN to the PS matrix. Figure 11 shows that the I3 nanocomposite has the highest refractive index of 4.2. Where, at $\lambda \geq 450$ nm, the refractive index values of the I1 sample decrease to 2.9 units and coincide with I3 at the wavelength period $375 \geq \lambda \geq 550$ nm, and the sample I2 has a value of 5.5 units, where the sample I2 has a refractive index value greater than the samples I1 and I3 at this wavelength period. This provides evidence that CNT and CN alter the PS structure when exposed to DBD plasma, which then rearranges the structure [30].

The extinction coefficient (*k*) for the PS nanocomposite thin films I0, I1, I2, and I3 is shown in Fig. 12. The extinction coefficient (*k*) is regarded as a very important parameter to describe the losses in absorption for the films. Therefore, it is dependent on the absorption coefficient (α) and the wavelength and can be calculated from equation 4 [31]:

$$k = \frac{\alpha\lambda}{4\pi} \ldots\ldots\ldots\ldots\ldots\ldots (4)$$

Thereby: (α) the absorption coefficient (cm^{-1}) and (λ) the wavelength in (cm).

Figure 12 shows the I0, I1, I2, and I3 curves of the PS nanocomposite films versus wavelength, with the corresponding extinction values.

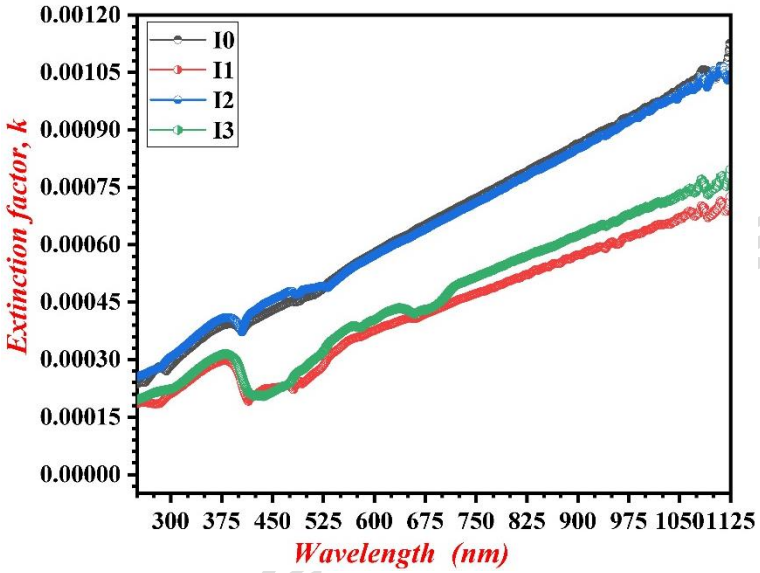

Figure 12. Extinction coefficient (k) of the PS nanocomposite films I0, I1, I2, and I3.

Figure 12 shows that the extinction factor is lower -quantified in parts per thousand- indicating minimal absorption losses. These values suggest that the nanocomposite films have a high absorption capacity, with losses diminishing considerably upon incorporation of CNT and CN and upon exposure of the samples to DBD plasma [32].

3.4. Dielectric constant of the nanocomposite films after exposure to DBD plasma

Analysis of the dielectric constant (Ɛ) provides critical insights into the electronic properties of the nanocomposite films. It reflects the material's capacity to store and dissipate electrical energy in response to an applied electric field, primarily through the polarization of electron dipoles. The real part of the dielectric constant ($Ɛ_r$) corresponds to

the energy stored in the material. In contrast, the imaginary part (ε_i) is associated with energy dissipation due to dielectric losses and represents wave attenuation within the medium. These components, ε_r and ε_i, are quantitatively evaluated using equation 5 [33]:

$$\begin{bmatrix} [(\varepsilon) = \varepsilon_r(\omega) + i\varepsilon_i(\omega)] \\ \varepsilon_r = n^2 - k^2 \\ \varepsilon_i = 2nk \end{bmatrix} \quad \text{..... (5)}$$

where: ε_r the real part and ε_i the imaginary part.

Thereby, the real dielectric constant (ε_r) for the PS nanocomposite films I0, I1, I2, and I3 curves are shown in Figure 13.

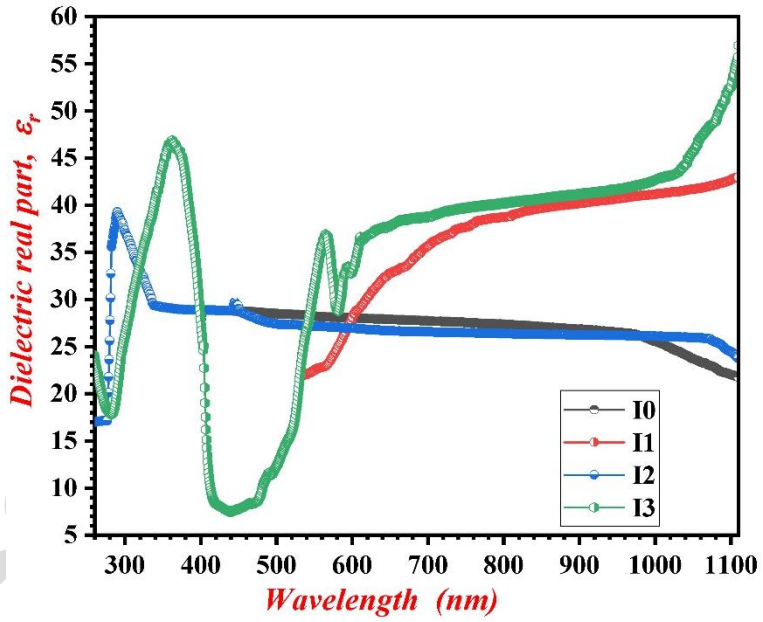

Figure 13. Real dielectric constant (ε_r) of the PS nanocomposite films I0, I1, I2, and I3.

Figure 13 illustrates the variation of the real dielectric constant (ε_r) as a function of wavelength for the PS nanocomposite films. The ε_r values exhibit pronounced maxima in the ultraviolet (UV) and near-visible regions (λ = 300-405 nm), reaching peak values of approximately 47, 40, and 47 for the samples I1, I2, and I3, respectively. Beyond this range ($\lambda \geq 400$ nm), ε_r progressively increases for the nanocomposites I1 and I3, attaining

values of 45 and 58, respectively. In contrast, for the nanocomposites I0 and I2, the values decrease to 21 and 22, respectively. Where, at $\lambda \geq 450$ nm, the real dielectric constant (ε_r) values of the I1 sample decrease to 8 units and coincide with I3 at the wavelength period $400 \geq \lambda \geq 580$ nm, where the sample I1 has a lower value of real dielectric constant (ε_r) at this wavelength period. The observed enhancement in ε_r is attributed to the incorporation of carbon nanotubes (CNTs) and carbon nanoparticles (CN) into the PS matrix, in conjunction with the dielectric barrier discharge (DBD) plasma treatment [34]. Figure 14 presents the corresponding trends for the imaginary part of the dielectric constant (ε_i) for the PS nanocomposite films I0, I1, I2, and I3, highlighting the dielectric loss behavior across the examined spectral range.

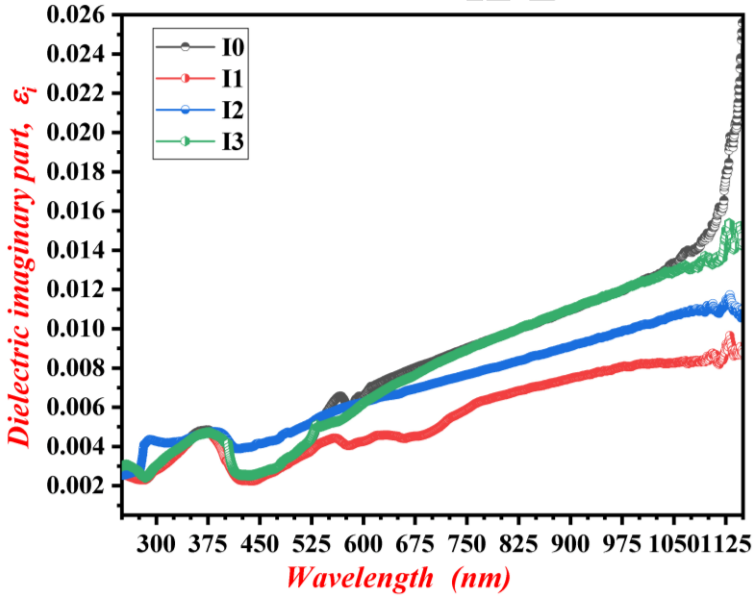

Figure 14. Imaginary dielectric constant (ε_r) of the nanocomposite films I0, I1, I2, and I3.

The imaginary part of the dielectric constant (ε_i) represents dielectric loss, which corresponds to the energy dissipated due to the restricted motion of electron dipoles within the material. As shown in Figure 14, the ε_i values for the nanocomposite films are relatively low, in the order of 10^{-4} or less, indicating minimal energy loss through

polarization. This suggests that the PS nanocomposite films exhibit strong optical absorption, facilitating the excitation of charge carriers from the valence band to the conduction band. The observed decrease in ε_i with increasing concentrations of carbon nanotubes (CNTs) and carbon nanoparticles (CN) in the PS matrix, particularly following dielectric barrier discharge (DBD) plasma treatment, further confirms improved optical and electronic performance of the films [35]. Furthermore, the optical conductivity (σ_{opt}) serves as a key parameter for evaluating the electrical response of the nanocomposite films under optical excitation. It is calculated using equation 6 [36]:

$$\sigma = \frac{\alpha nc}{4\pi} \quad \text{..... (6)}$$

where σ_{opt} is the optical conductivity (S^{-1}), α is the absorption coefficient (cm^{-1}), nnn is the refractive index, and c is the speed of light in vacuum (3×10^{10} cm/s).

The optical conductivity (σ_{opt}) curves for the PS nanocomposite samples I0, I1, I2, and I3 are shown in Figure 15, revealing the influence of CNT and CN incorporation on the films' optoelectronic properties.

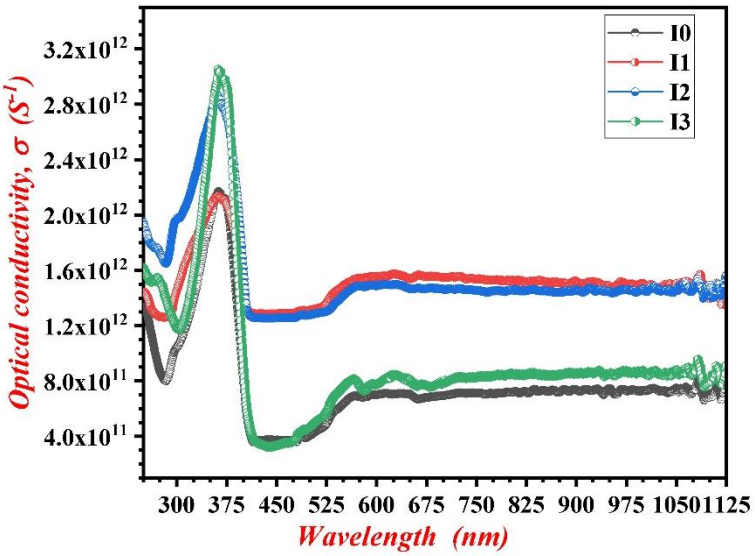

Figure 15. Optical conductivity (σ_{opt}) of the PS nanocomposite films I0, I1, I2, and I3.

As shown in Figure 15, the optical conductivity ($Ϭ_{opt}$) exhibits a significant increase following the incorporation of carbon nanotubes (CNTs) and carbon nanoparticles (CN) into the PS matrix. The $Ϭ_{opt}$ values range from approximately 4.0×10^{11} to 3.1×10^{12} S^{-1}, indicating enhanced charge carrier mobility and improved optoelectronic behavior. Beyond the initial rise, the conductivity curves remain relatively stable as the wavelength increases, suggesting a consistent optical response across the measured spectral range. The observed enhancement in $Ϭ_{opt}$ is attributed to the synergistic effects of CNT and CN incorporation, as well as the surface modification induced by dielectric barrier discharge (DBD) plasma treatment [37].

3.5. Energy gap of the nanocomposite films after exposure to DBD plasma

The optical energy band gap (E_g) is a fundamental parameter that characterizes the semiconducting behavior of nanocomposite thin films. It can be determined using Tauc's equation 7 [38]:

$$\alpha h\nu^{r} = B(h\nu - E_g) \quad \text{..... (7)}$$

where α is the absorption coefficient, hν is the photon energy, B is a material-dependent constant, and r represents the nature of the electronic transition (r=0.5 for indirect allowed transitions and r=2 for direct allowed transitions).

The energy gap (E_g) is estimated by extrapolating the linear portion of the r(αhν)^r vs. hν plot to the photon energy axis, where (αhν)^r = 0.

A larger energy gap indicates fewer electronic transitions between the valence and conduction bands, resulting in lower electrical conductivity. Figure 16 presents the direct energy gap values for the PS nanocomposite films labelled I0, I1, I2, and I3.

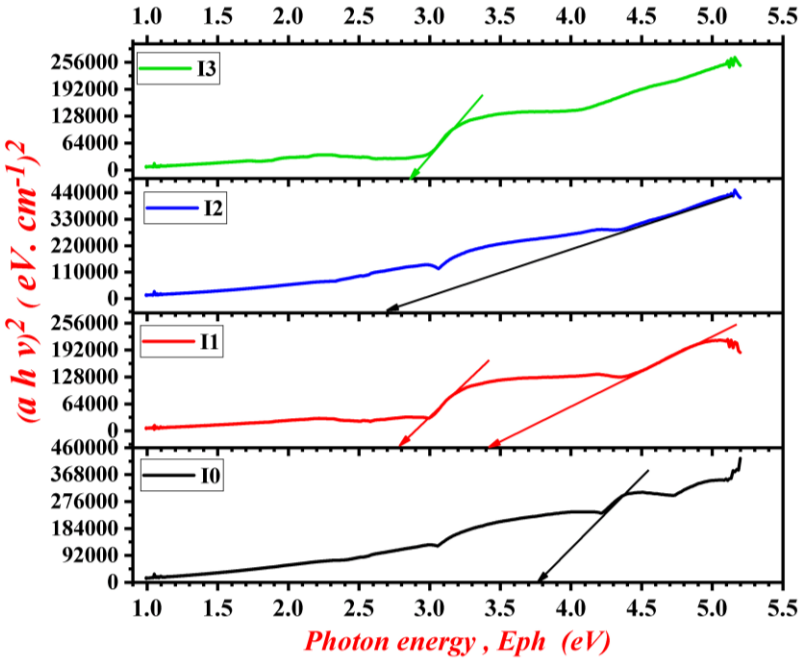

Figure 16. Direct energy gap (E_g) of the PS nanocomposite films I0, I1, I2, and I3.

As shown in Figure 16, the blank PS (I0) exhibits a band gap of approximately 3.8 eV. The nanocomposite samples exhibit a slight reduction in E_g, with values of 3.4 and 2.8 eV for I1. The E_g The energy of I2 is equal to 2.7 eV, and 2.9 eV for I3. These variations suggest structural modifications and particle rearrangements in the PS matrix upon incorporation of carbon nanotubes (CNTs) and carbon nanoparticles (CN), especially under dielectric barrier discharge (DBD) plasma treatment. The observed reductions in band gap are consistent with enhanced optical absorption, indicating that the nanocomposite films exhibit semiconductor-like behavior [39]. Figure 17 shows the indirect energy gaps for the PS nanocomposite films labelled I0, I1, I2, and I3.

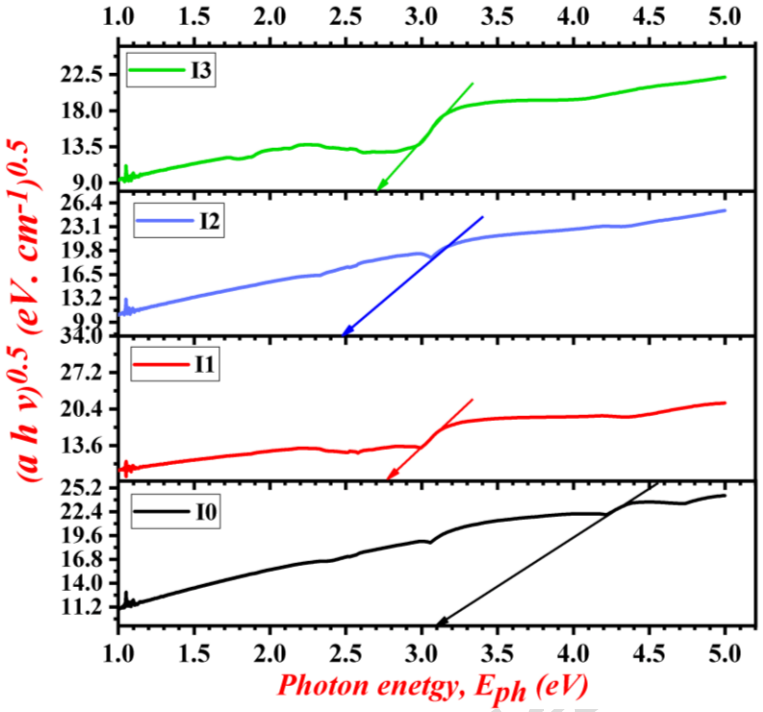

Figure 17. Indirect energy gap (E_g) of the PS nanocomposite films I0, I1, I2, and I3.

Similarly, Figure 17 illustrates the indirect energy gap (E_g) values for the same film samples. The blank PS (I0) exhibits an indirect band gap of approximately 3.1 eV, while the modified samples display lower values: 2.8 eV for I1, 2.5 eV for I2, and 2.7 eV for I3. These closely spaced values imply a consistent modification of the polymeric structure across the samples, attributed to the synergistic effects of CNT and CN additives in conjunction with DBD plasma exposure. This structural rearrangement enhances the optical properties and further supports the semiconducting nature of the treated PS nanocomposite films [40].

3.6. Urbach energy of the nanocomposite films after exposure to DBD plasma

Urbach energy (E_g) is an important parameter used to assess the degree of structural disorder in both crystalline and amorphous materials. It reflects the width of the band tail

of localized states within the energy gap and is indicative of imperfections and disordered arrangements in the material. The Urbach energy can be calculated using the following empirical relation (Eq. 8) [41]:

$$\alpha = \alpha_o exp\frac{h\nu}{E_u} \ldots\ldots\ldots\ldots\ldots\ldots\ldots \quad (8)$$

where α is the absorption coefficient, α is a material-specific constant, hν is the photon energy, and E_u is the Urbach energy (in eV). Taking the natural logarithm of both sides of equation 8 yields a linearized form (Eq. 9):

$$ln\ \alpha = ln\ \alpha_o + \frac{h\nu}{E_u} \ldots\ldots\ldots\ldots\ldots\ldots\ldots \quad (9)$$

This expression allows for the determination of Eu from the slope of the linear region of the ln(α) versus hν plot. Figure 18 presents the Urbach energy values for the PS nanocomposite thin films labelled I0, I1, I2, and I3, illustrating the effect of carbon nanotube (CNT) and carbon nanoparticle (CN) incorporation, along with dielectric barrier discharge (DBD) plasma treatment, on the degree of structural disorder within the material.

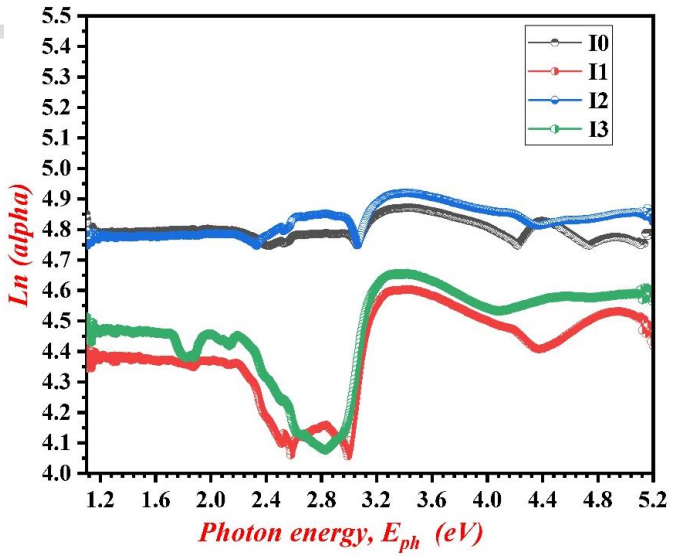

Figure 18. Urbach energy (E_u) of the PS nanocomposite films P0, P1, P2, and P3.

As illustrated in Figure 18, the Urbach energy (E_u) increases with increasing wavelength for the I0, I1, I2, and I3 nanocomposite films, ranging from 0.0232 meV to 0.0877 meV. This rise in E_u Indicates an enhancement in the degree of structural disorder within the PS nanocomposite thin films. A higher Urbach energy (E_u) corresponds to a greater density of localized states in the band gap, facilitating electronic transitions by enabling charge carriers to overcome potential barriers and move from the valence to the conduction band. This behavior results in an increase in charge carrier density and improved electrical conductivity [42].

Simultaneously, the absorption coefficient pre-exponential factor ($\alpha_\circ$) also increases from 76.32 cm^{-1} to 121.15 cm^{-1}, supporting the observation of enhanced light absorption. These findings confirm that the PS nanocomposite films exhibit semiconducting behavior, characterized by strong absorption and high optical conductivity in response to incident light [42]. A comprehensive summary of the energy gap and Urbach energy values for all film samples is presented in Table 3.

Table 3. Results of the energy gap and the Urbach energy for the PS nanocomposite films

No.	Parameters	Blank PS	PS +5% CNT	PS +5% CN	PS +2.5% CNT+CN
1	Direct transition of (E_g) (eV)	3.8	3.4 and 2.8	2.7	2.8
2	Indirect transition of (E_g) (eV)	3.1	2.8	2.5	2.7
3	Urbach energy (E_u) meV	0.0232	0.0571	0.0388	0.0877
4	(α_0) absorption constant **(**cm^{-1}**)**	76.32	121.15	115.35	83.35

3.7. Urbach energy (E_u) and energy gap (E_g) relation for films of PS

Figure 19 shows the relation between the Urbach energy (E_u) and energy gap (E_g) for the PS nanocomposite films I0, I1, I2, and I3. It shows the behavior of the Urbach energy (E_u) versus energy gap (E_g) values, the Eu values increased after E_g decreased, as shown in Figure 20.

Therefore, this demonstrates that these PS nanocomposite films exhibit significant light absorption and conductivity [43].

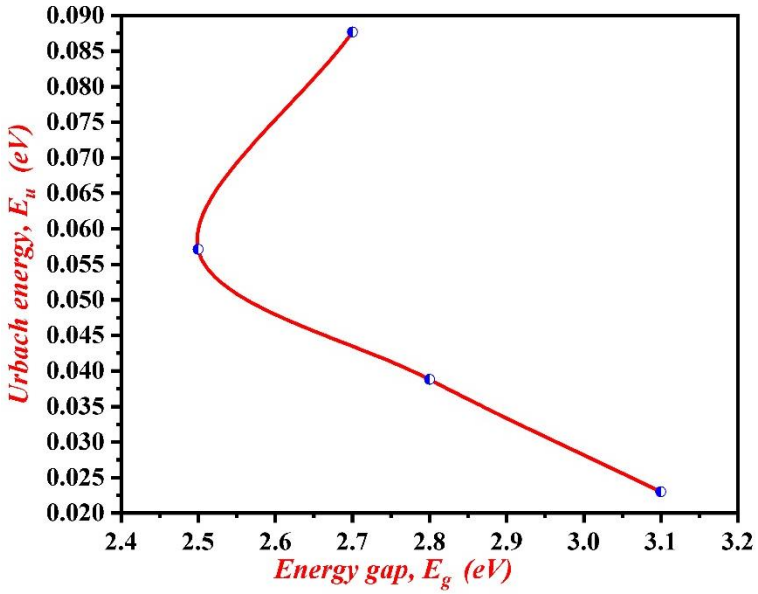

Fig. 19. Urbach energy (E_u) versus energy gap (E_g).

3.8. SEM analysis of the PS nanocomposite films

The surface morphology of the PS nanocomposite thin films was investigated using scanning electron microscopy (SEM), with each film prepared using different concentrations of carbon nanotubes (CNTs) and carbon nanoparticles (CN). The compositions are as follows: I0 represents the blank PS (blank sample), I1 contains PS with 5 wt.% CNT, I2 contains 5 wt.% CN, and I3 contains a hybrid mixture of PS with 2.5 wt.% CNT and 2.5 wt.% CN. The SEM micrographs for these samples are presented in Figure 20.

As shown in Figure 20a, the surface of the blank PS (I0) is relatively smooth, exhibiting only minor particulates that appear as white spots, which are attributed to slight phase immiscibility, upon incorporation of 5 wt.% CNT (I1, Figure 20b), a modest increase in

surface roughness is observed, along with the formation of small clusters and the emergence of pores. This indicates that CNTs begin to integrate into the PS matrix without forming extensive aggregation at this concentration.

In contrast, the addition of 5 wt.% CN (I2, Figure 20c) results in more pronounced surface roughness and visible aggregation of CN particles. Although the dispersion is somewhat sparse, pore formation is still evident. The most significant morphological changes are observed in the hybrid composite (I3, Figure 20d), where a mixture of 2.5 wt.% CNT and 2.5 wt.% CN leads to substantial surface roughness, increased clustering, and noticeable agglomeration. The distribution of CNT and CN appears more uniform and denser, significantly altering the PS matrix structure. The resulting morphology is characterized by large clusters, higher porosity, and a dominant particulate dispersion, suggesting surface saturation with nanofillers. The increased roughness and the appearance of white spots are attributed to both the high loading of nanomaterials and partial immiscibility within the polymer matrix [44-46].

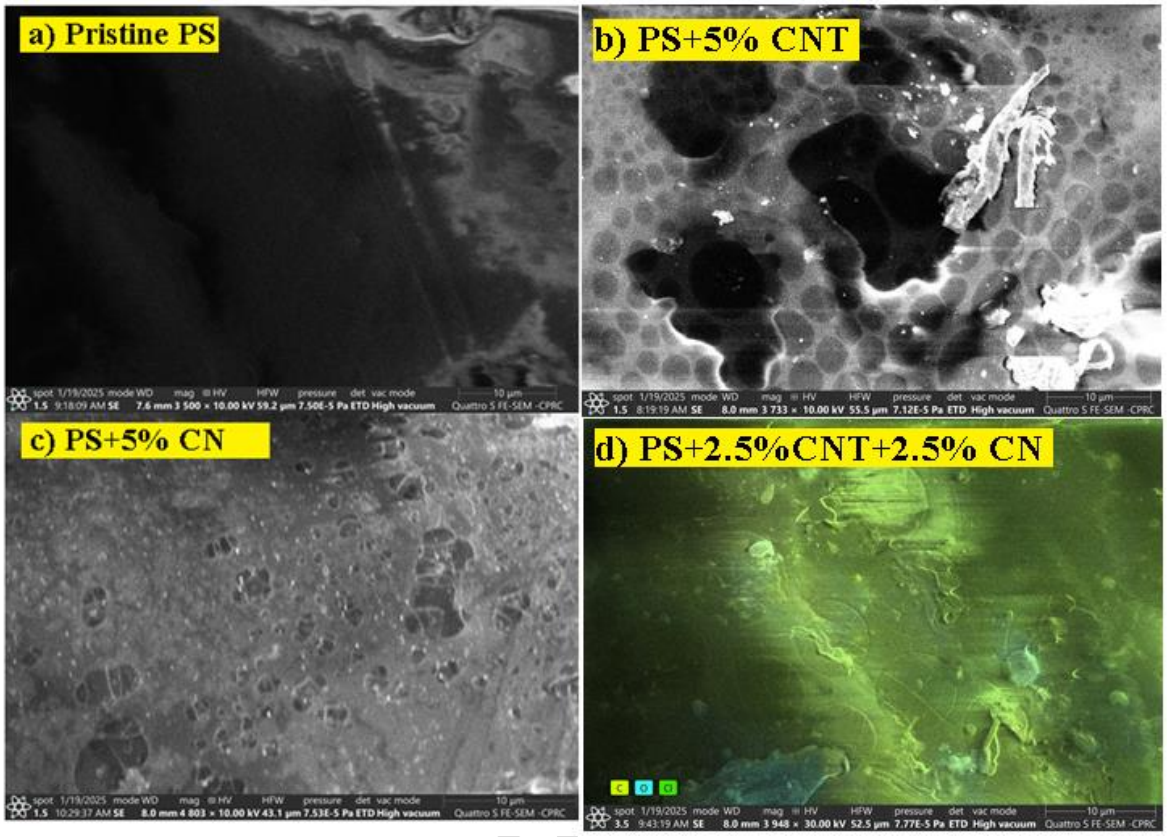

Figure 20. SEM images: a) PS blank, b) PS +5% CNT, c) PS +5% CN, and d) PS +2.5% CNT+2.5 % CN.

3.9. AFM analysis

Atomic Force Microscopy (AFM) was employed to characterize the surface morphology of the PS nanocomposite thin films, providing both two-dimensional (2D) and three-dimensional (3D) topographical images. This technique offers high-resolution surface analysis and is particularly effective for detecting morphological variations that influence the optical and electronic properties of materials, especially in response to incident light. Numerous studies have demonstrated the utility of AFM in evaluating nanoscale surface features and roughness in polymer-based nanocomposites.

Figure 21 presents AFM images of pristine and modified PS films to investigate the effect of incorporating carbon nanotubes (CNTs) and carbon nanoparticles (CN) on

surface roughness. The analysis reveals quantitative surface roughness (SR) and root-mean-square (RMS) values of 4.06 nm and 5.66 nm, respectively, for the pristine PS film (I0, Figure 21a). Upon the addition of 5 wt.% CNT (I1, Figure 21b), the same values 4.06 nm (SR) and 5.30 nm (RMS). Similarly, the film with 5 wt.% CN (I2, Figure 21c) exhibited SR and RMS values of 9.28 nm and 11.90 nm, respectively. The hybrid composite containing 2.5 wt.% CNT and 2.5 wt.% CN (I3, Figure 21d) demonstrated the highest surface roughness, with SR and RMS values of 6.03 nm and 8.14 nm, respectively.

These results suggest that incorporating CNT and CN, either individually or in combination, significantly alters the surface texture of the PS films, increasing their roughness and potentially improving their interaction with light and charge carriers. A detailed summary of SR and RMS values for all samples is provided in Table 4 [47-51].

Table 4. Characterization of the roughness of PS films with the AFM technique

No.	Composite	Number of Figures	Roughness average (SR) (nm)	Root mean square of roughness (RMS) (nm)
1	PS-blank (I0)	21a	4.06	5.66
2	PS+5% CN (I1)	21b	4.06	5.30
3	PS+5% CNT (I2)	21c	9.28	11.90
4	PS+ PS+2.5% CN+2.5% CNT (I3)	21d	6.03	8.14

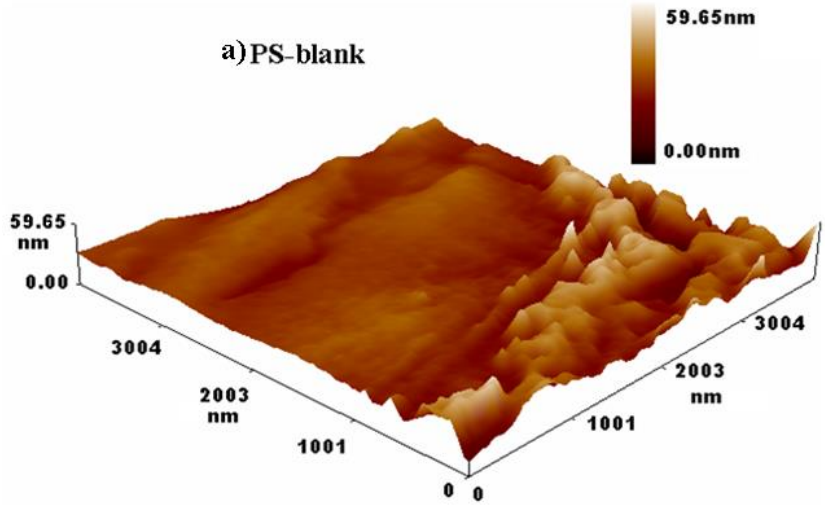

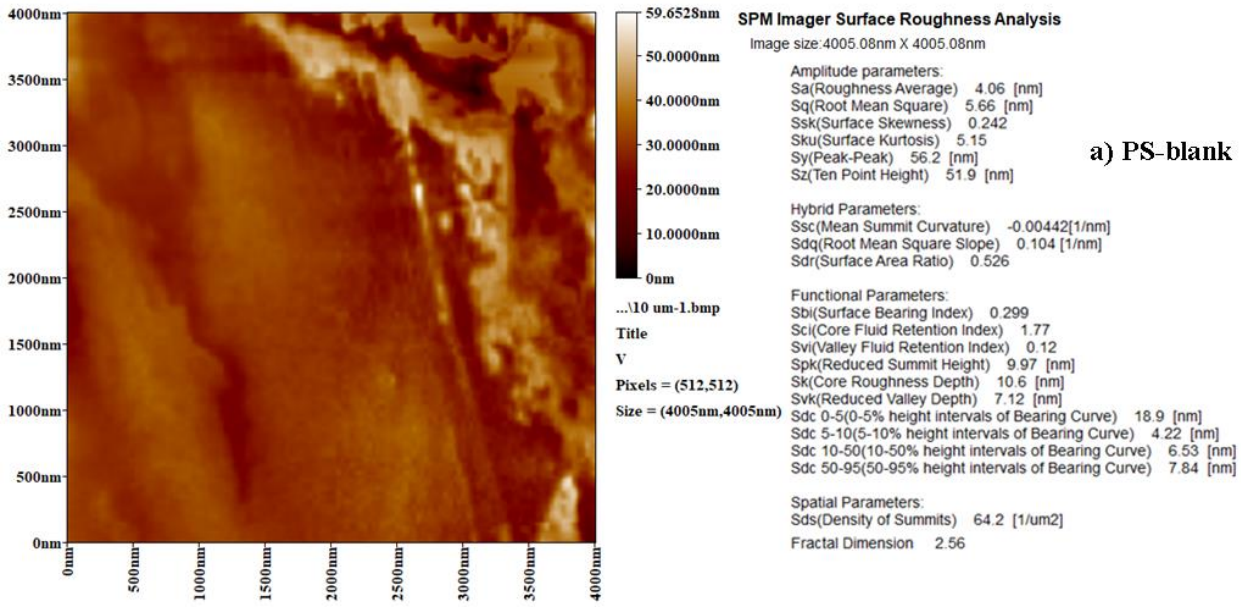

a) PS-blank

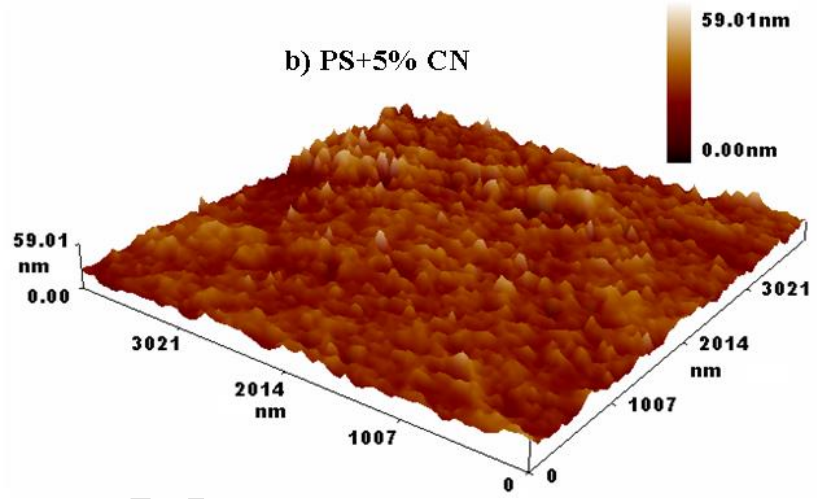

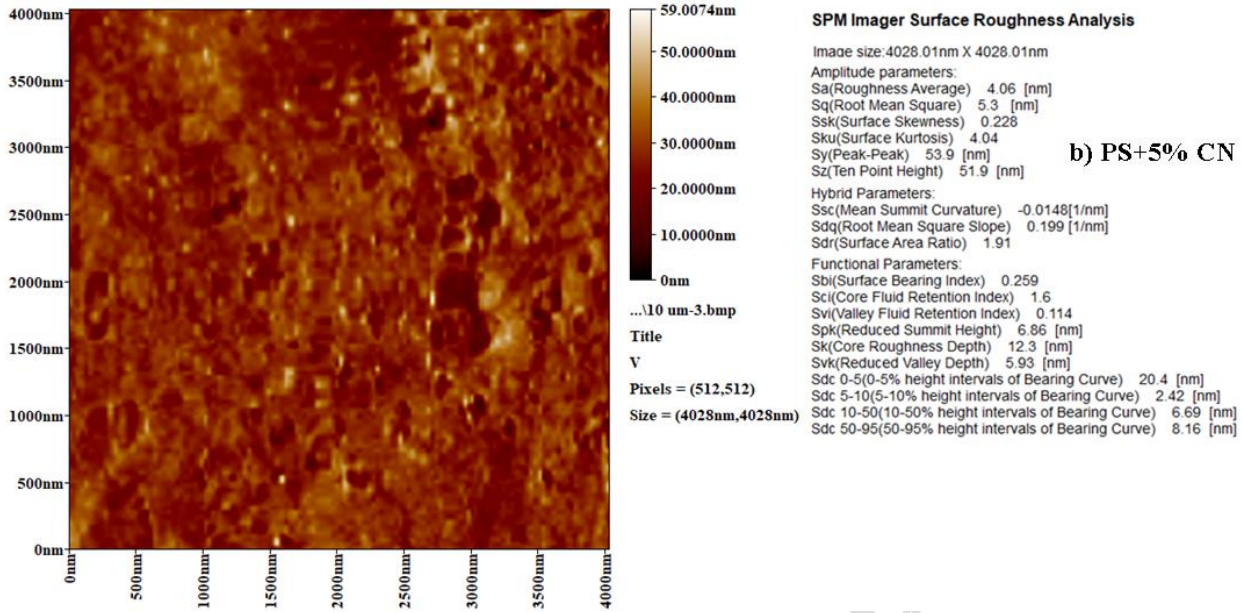

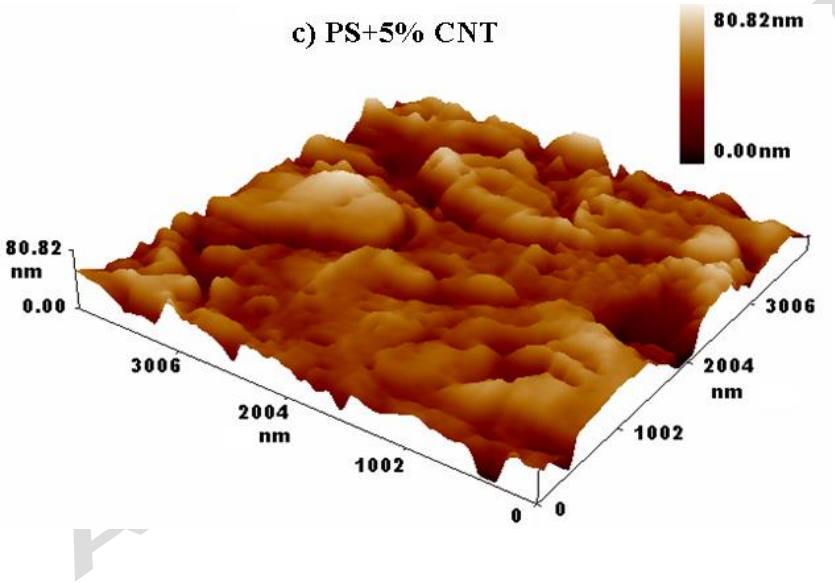

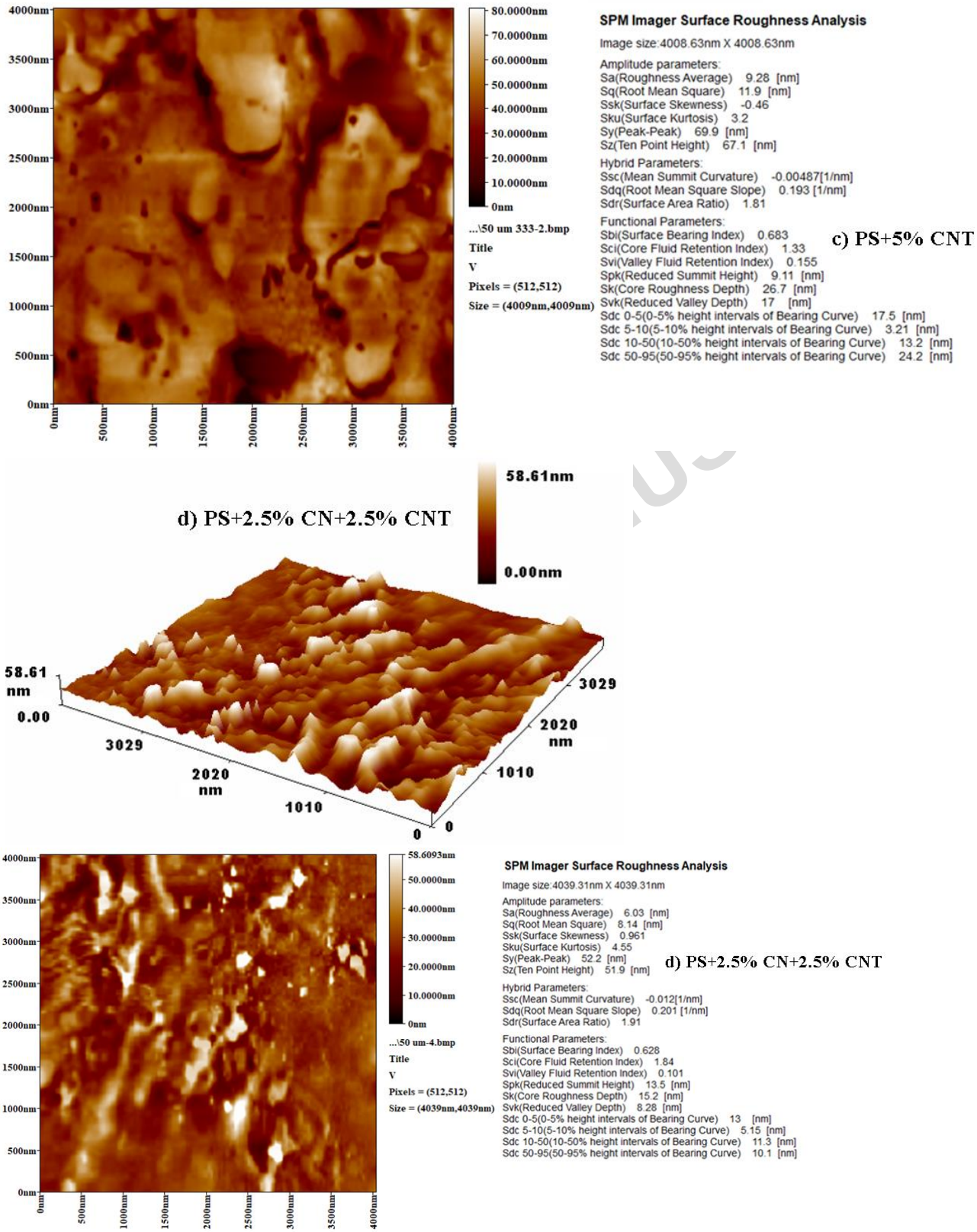

Figure 21. AFM images for: a) PS blank, b) PS+5% CNT, c) PS+5% CN, and d) PS+2.5% CNT+2.5CN

4. Conclusions

The new spectrally nanocomposite thin films of the nano coatings have been developed to achieve high absorption performance. A 1.0 g constant rate of polystyrene (PS) dissolved in 100 ml THF, after that the solution splits into three parts to blende with fixed concentrations of carbon nanotube (5% CNT) as the first part, carbon nano (5 wt. % CN) as a second part, and (2.5% CNT+2.5% CN) as a third part via casting technique to make PS nanocomposite films. The CNT and CN incorporated into the PS matrix to form the nanocomposite films have been developed to create economical coatings used extensively in many applications. The nano coating exhibits high light absorption, and its optical properties have been studied over 250-1350 nm at room temperature (30 °C). The transmittance and reflectance decreased, but the skin depth and optical density increased; additionally, the absorbance coefficient and dielectric constant rose following the incorporation of CNT and CN. The direct and indirect energy gap (E_g) of the nanocomposite films has been decreased from 3.8 to 2.7 eV and from 3.1 to 2.5 eV after adding CNT with CN, consequently. The increases in Urbach energy (E_u) have been observed, and its value increased from 0.0232 to 0.0877 meV due to an increase in the localized states between the valence and conduction bands. The XRD analysis confirms that the nanocomposite films are amorphous. The SEM analysis was used to visualize the surface morphology of the thin films before and after the addition of CNT with CN. The AFM analyses provided visual evidence of the doped PS nanocomposite structure and increased roughness (SR) from 4.06 to 9.28 nm, and the root-mean-square (RMS) increased from 5.3 to 11.90 nm. These modified PS nanocomposite thin films hold potential for various industrial applications, including air transport, light-emitting diodes,

laser sensors, UV shields, light harvesting, memory devices, and light-converting devices.

Acknowledgments

This research was facilitated by the Department of Mechanical Engineering in the College of Engineering and the Department of Chemistry in the College of Science at Al-Nahrain University, which provided access to laboratory facilities.

Conflict of Interest

The authors assert that there is no conflict of interest among them in this work.

Funding Information

This manuscript received no funding; it was solely financed by the authors, who incurred all associated expenses.

References

1. Paul A, Grady B, Ford W. Polystyrene composites of single-walled carbon nanotubes-graft-polystyrene. Poly Inter. 2012; 61:1603–10. https://doi.org/10.1002/pi.4258
2. Mittal V., Polymer nanotube nanocomposites: synthesis, properties, and applications. Wiley pub., 2024. https://doi.org/10.1002/9781118945964

3. Liu Y, Wang G, Wu Y. Amphiphilicity and self-assembly behaviors of polystyrene-grafted multi-walled carbon nanotubes in selective solvents. Colloid Polym Sci. 2014; 292:185-96. https://doi.org/10.1007/s00396-013-3066-y
4. Iijima S., Helical microtubules of graphitic carbon. Nature. 1991; 354:56-8. https://doi.org/10.1038/354056a0
5. Suhr J, Victor P, Ci L, Sreekala S, Zhang X, Nalamasu O. Fatigue resistance of aligned carbon nanotube arrays under cyclic compression. Nat Nanotechnol. 2007; 2:417-21. https://doi.org/10.1038/nnano.2007.186
6. Chehata N, Ltaief A, Bkakri R, Bouazizi A, Beyou E. Conducting polymer-functionalized multi-walled carbon nanotubes nanocomposites: optical properties and morphological characteristics. Mater Lett. 2014; 121:227-30. https://doi.org/10.1016/j.matlet.2014.01.162
7. Ismail RA, Almashhadani NJ, Sadik RH. Preparation and properties of polystyrene incorporated with gold and silver nanoparticles for optoelectronic applications. Appl Nanosci. 2017; 7:109-16. https://doi.org/10.1007/s13204-017-0550-6
8. Yang J, Zhang Z, Men X, Xu X. Fabrication of stable, transparent and superhydrophobic nanocomposite films with polystyrene functionalized carbon nanotubes. Appl Surf Sci. 2009; 255:9244-7. https://doi.org/10.1016/j.apsusc.2009.07.010
9. Al-Taa'y WA, Ibraheem H, Yousif E, Jelassi H. Studies on surface morphology and electrical conductivity of PS thin films in the presence of divalent complexes. Baghdad Sci J. 2019; 16:588-94. https://doi.org/10.21123/bsj.2019.16.3.0588

10. Mezan SO, Jabbar AH, Hamzah MQ, Tuama AN, Hasan NN, Roslan MS, Agam MA. Synthesis, characterization, and properties of polystyrene/SiO_2 nanocomposite via sol–gel process. AIP Conf Proc. 2019; 2151:020034-1–020034-7. https://doi.org/10.1063/1.5124664
11. Doğuscü DK, Hekimoğlu G, Sari A. High internal phase emulsion templated-polystyrene/carbon nanofiber/hexadecanol composites phase change materials for thermal management applications. J Energy Storage. 2021; 39:102674. https://doi.org/10.1016/j.est.2021.102674
12. Kumar M. S. S., Selvan C. P., Santhanam K., Kadirvel A., Chandraprabu V., SampathKumar L., Effect of nanomaterials on tribological and mechanical properties of polymer nanocomposite materials. Adv. Mater. Scien. Eng. 2022; 2165855:1-16. https://doi.org/10.1155/2022/2165855
13. Farag O F, Abdel-Fattah E S. Synthesis and characterization of PVA/plasma-functionalized MWCNTs nanocomposites films. J Polym Res. 2023; 30:183. https://doi.org/10.1007/s10965-023-03550-8
14. Kumar D, Amika, Kumar D, Singh P, Chauhan AS, Kapoor S, Bansal SA. Polymer/carbon nanotube composites: A comprehensive review on fabrication techniques and their consequences. AIMS Mater Sci. 2025;12(4):813-44. https://doi.org/10.3934/matersci.2025035.
15. Morent R, De Geyter N, Leys C, Gengembre L, Payen E. Non-thermal plasma treatment of textiles. Surf Coat Technol. 2008; 202(14):3427-49. https://doi.org/10.1016/j.surfcoat.2007.12.027

16. Friedrich J. Mechanisms of plasma polymerization reviewed from a chemical point of view. Plasma Process Polym. 2011; 8(9):783-802. https://doi.org/10.1002/ppap.201100038.

17. Abdulwahid AA, Alwan LH, Ahmed AA, Abed RN. Optical and physical properties for the nanocomposite poly(vinyl chloride) with affected of carbon nanotube and nano carbon. Prog Color Colorants Coat. 2023;16(4):329-38. https://doi.org/10.30509/PCCC.2023.167082.1198

18. Patel V, Joshi U, Joshi A, Matanda B K, Chauhan K, Oza A D, Nergis D P B, and Nergis D D B, Multi-Walled Carbon-Nanotube-Reinforced PMMA Nanocomposites: An Experimental Study of Their Friction and Wear Properties. Polymers 2023; 15(13): 2785; https://doi.org/10.3390/polym15132785

19. Li J-W, He Y-L, Chen L-W, Luo X-Z, Cao D-X, Tan Y-C. Photocurable carbon nanotube/polymer nanocomposite for the 3D printing of flexible capacitive pressure sensors. Polymers. 2023; 15(24):4706. https://doi.org/10.3390/polym15244706

20. Kausar A, Ahmad I. Electrospinning processing of polymer/nanocarbon nanocomposite nanofibers: design, features, and technical compliances. J Compos Sci. 2023;7(7):290. https://doi.org/10.3390/jcs7070290

21. El-Naggar AM. Optical and dielectric features of PVC/$ZnCo_2O_4$/MWCNTs/TBAI polymers for optoelectronic and energy storage applications. Inorg Chem Commun. 2023; 152:111624. https://doi.org/10.1016/j.inoche.2023.111624

22. Yang CC, Tsai JS, Chuang YC, Hsu YC. Enhancing the photoelectric properties of flexible carbon nanotube paper by plasma gradient modification and gradient illumination. Processes. 2024; 12(7):1449. https://doi.org/10.3390/pr12071449

23. Alkhursani, S.A., Aldaleeli, N., Elbasiony, A.M. et al. Simulation and characterization of Co_3O_4/carbon nanotube-filled PVC nanocomposites for medium-voltage cable applications. Polym. Bull. 81, 15841-15864 (2024). https://doi.org/10.1007/s00289-024-05435-2

24. Abdullah AM, Alwan LH, Ahmed AA, et al. Optical properties of polystyrene with carbon nanotube and carbon nano incorporated and surface morphology studies. Int Nano Lett. 2023; 13:165-76. https://doi.org/10.1007/s40089-023-00398-0

25. Liu T W, Zhao Z, Cao R, Liu Y Y, Jiang X, Reliability challenges of gate dielectric materials in transistors. Inform. Function. Mater. 2025; 2(1):62-92. https://doi.org/10.1002/ifm2.31

26. Abed R. N., Yousif E., Abed A. R. N., Rashad A. A., Hadawey A., Jawad A. H. Optical properties of PVC composite modified during light exposure to give high absorption enhancement. J. Non-Crys. Solids 2021; 570:120946. https://doi.org/10.1016/j.jnoncrysol.2021.120946

27. Abed R. N., Abed A. R. N., F. A. Khamas, Abdallh M., Yousif E. High performance thermal coating comprising (CuO:NiO) nanocomposite/C spectrally selective to absorb solar energy. Prog Color Colorant Coat. 2020; 13:275-284. https://doi.org/10.30509/PCCC.2020.81662

28. Abed RN, Abdallh M, Rashad AA, Hadawey A, Yousif E., New coating synthesis comprising CuO:NiO/C to obtain highly selective surface for enhancing solar energy absorption. J Polym Bull. 2021; 78:433-455. https://doi.org/10.1007/s00289-020-03115-5

29. Abed R N, Kadhom M, Ahmed D S, Hadawey A, Yousif E. Enhancing optical properties of modified PVC and Cr_2O_3 nanocomposite. Trans Electr Electron Mater. 2021; 22:317-327. https://doi.org/10.1007/s42341-020-00242-8

30. Urbach F. The long wavelength edge of photographic sensitivity and of the electronic absorption of solids. Phys Rev. 1953; 92:1324. https://doi.org/10.1103/PhysRev.92.1324

31. Abed RN, Yousif E, Abed ARN, Rashad AA. Synthesis thin films of poly(vinyl chloride) doped by aromatic organosilicon to absorb the incident light. Silicon. 2022; 14:11829-11845. https://doi.org/10.1007/s12633-022-01893-3

32. Abdullah OG, Saber DR. Optical absorption of poly(vinyl alcohol) films doped with nickel chloride. Appl Mech Mater. 2012; 110-116:177-82. https://doi.org/10.4028/www.scientific.net/AMM.110-116.177

33. Zhang Q, Liang W, Xiong L, Wang Y, Xu H. A polymer nanocomposite with strong full-spectrum solar absorption and infrared emission for all-day thermal energy management and conversion. Adv Sci. 2024; 11(8):e202308200. https://doi.org/10.1002/advs.202308200

34. Dolai S, Sarangi SN, Hussain S, Bhar R, Pal AK. Magnetic properties of nanocrystalline nickel incorporated CuO thin films. J Magn Magn Mater. 2019; 479:59-66. https://doi.org/10.1016/j.jmmm.2019.02.005

35. Abdullah AM, Alwan LH, Ahmed AA, Abed RN. Physical study of PVA filled with carbon nanotube and nano carbon with roughness morphology. J Phys Chem Res. 2023; 11:747-60. https://doi.org/10.22036/PCR.2022.362088.2195

36. Abed RN, Al-Sahib NK, Khalifa AJN. Energy gap demeanor for carbon doped with chrome nanoparticle to increase solar energy absorption. PCCC. 2020; 13:143-54. https://doi.org/10.30509/PCCC.2020.81613

37. Al-Bataineh QM, Alsaad AM, Ahmad AA, Al-Sawalmih A. Structural, electronic and optical characterization of ZnO thin film-seeded platforms for ZnO nanostructures: sol–gel method versus ab initio calculations. J Electron Mater. 2019; 48:5028-38. https://doi.org/10.1007/s11664-019-07303-6.

38. Pankove JI. Optical processes in semiconductors. New York: Dover Publications; 1975. p. 91.

39. Ahmed A, Abed RN, Kadhom M, Hashim H, Akram E, Jawad A, et al. Modification of poly(vinyl chloride) thin films with organic compound and nanoparticles for solar energy applications. J Polym Res. 2023; 30:36. https://doi.org/10.1007/s10965-023-03654-1

40. Abed RN, Yousif E, Abed ARN, Rashad AA. Synthesis of thin films of poly(vinyl chloride) doped by aromatic organosilicon to absorb the incident light. Silicon. 2022; 14:11829-45. https://doi.org/10.1007/s12633-022-01893-3

41. Abed RN, Al-Mashhadani MH, Yousif E, Hashim H, Yusop RM, Bufaroosha M. Organosilane-doped PVC lattice thin film for optoelectronic applications. J Opt. 2023; https://doi.org/10.1007/s12596-023-01351-2

42. Fasasi A, Osagie E, Pelemo D, Obiajunwa E, Ajenifuja E, Ajao J, et al. Effect of precursor solvents on the optical properties of copper oxide thin films deposited using spray pyrolysis for optoelectronic applications. Am J Mater Synth Process. 2018; 3(2):12-22. https://doi.org/10.11648/j.ajmsp.20180302.12

43. Zanatta AR. Revisiting the optical bandgap of semiconductors and the proposal of a unified methodology. Sci Rep. 2019; 9:11225. https://doi.org/10.1038/s41598-019-47670-y

44. Alsaad AM, Al-Bataineh QM, Ahmad AA, Albataineh Z, Telfah A. Optical band gap and refractive index dispersion parameters of boron-doped ZnO thin films: a novel derived mathematical model from the experimental transmission spectra. Optik. 2020; 211:164641. https://doi.org/10.1016/j.ijleo.2020.164641

45. Abdullah AM, Alwan LH, Ahmed AA, Abed RN. Optical and physical properties for the nanocomposite poly(vinyl chloride) with affected of carbon nanotube and nano carbon. Prog Color Colorants Coat. 2023; 16:331-45. https://doi.org/10.30509/PCCC.2023.167082.1198

46. Hassanien AS, Akl AA. Effect of Se addition on optical and electrical properties of chalcogenide CdSSe thin films. Superlattices Microstruct. 2016; 89:153-69. https://doi.org/10.1016/j.spmi.2015.10.044

47. Abed ARN, Abed RN. Characterization effect of copper oxide and cobalt oxide nanocomposite on poly(vinyl chloride) doping process for solar energy applications. PCCC. 2022; 15:235-41. https://doi.org/10.30509/PCCC.2021.166858.1123

48. Emir P, Kuru D. Boron nitride quantum dots/polyvinyl butyral nanocomposite films for the enhanced photoluminescence and UV shielding properties. J Appl Polym Sci. 2024; 141:55171. https://doi.org/10.1002/app.55171

49. Abed R. N., Zainulabdeen K., Abdallh M., Yousif E., Rashad A. A., Jawad A. H. The optical properties behavior of modify poly(methyl methacrylate) nanocomposite thin films during solar energy absorption. J Non-Cryst Solids 2023; 609:122257. https://doi.org/10.1016/j.jnoncrysol.2023.122257

50. Dadoosh R. M., Alwan A. F., Farhan S. A., Jassim B. E., Mahmood A., Al-Saadi L. G., et al. Study of Physicochemical Properties of PVC Thin Films Affected by Carbon Nanotubes to Prevent Photodegradation During UV Light Exposure. Prog Color Colorant Coat. 2024; 17:307-324. https://doi.org/ 10.30509/pccc.2024.167260.1275

51. Abed RN, Rashad AA, Rahman MH, Basem A, Al-Ani A, Husain A, Jumaah NS, Hashim H, Bufaroosha MS, Yousif E, Hadawey A: Synthesis, structural, and optical properties of modified poly(vinyl chloride) thin films by ethylenediamine loaded with metal oxide nanoparticles. chemistrySelect: 2024; 9:1-17. https://doi.org/10.1002/slct.202401717